Research Article | Vol. 27, No. 26 / 23 December 2019 / Optics Express 37652
Optics EXPRESS

Using Bessel beams and two-photon absorption to predict radiation effects in microelectronics

JOEL M. HALES,[1,2,5] ANI KHACHATRIAN,[1] JEFFREY WARNER,[1] STEPHEN BUCHNER,[1] ADRIAN ILDEFONSO,[3] GEORGE N. TZINTZAROV,[3] DELGERMAA NERGUI,[3] DANIELE M. MONAHAN,[4] STEPHEN D. LALUMONDIERE,[4] JOHN D. CRESSLER,[3] AND DALE MCMORROW[1,6]

[1]*Electronics Science and Technology Division, U.S. Naval Research Laboratory, Washington, DC 20375, USA*
[2]*KeyW Corporation, Herndon, VA 20171, USA*
[3]*School of Electrical and Computer Engineering, Georgia Institute of Technology, Atlanta, GA 30332-0250, USA*
[4]*The Aerospace Corporation, Los Angeles, CA 90009-2957, USA*
[5]*joelmh@hotmail.com*
[6]*dale.mcmorrow@nrl.navy.mil*

Abstract: Pulsed-laser testing is an attractive tool for studying space-based radiation effects in microelectronics because it provides a high degree of spatial resolution and is more cost-effective than conventional accelerator-based testing. However, quantitatively predicting the effects of radiation is challenging for this optical method. A new approach to pulsed-laser testing is presented, which addresses these challenges by using a Bessel beam and carrier generation via two-photon absorption. By producing a carrier distribution in the device under test that is similar to that of a heavy ion, this optical approach aims to quantitatively predict the response of the device under heavy ion tests that represent space radiation. Furthermore, the carrier distribution can be accurately described using a single analytic expression thereby enabling the laser to be tuned to emulate a specific heavy ion. Herein, we describe the modifications made to an existing pulsed-laser setup to generate this carrier distribution, characterize this distribution using a novel method that provides sub-micron spatial resolution, and provide the equations that describe the distribution. Finally, we use this method to study a silicon photodiode and find that the transient response of the device shows strong agreement with the response generated using heavy ions.

1. Introduction

Radiation-induced phenomena, in particular, those referred to as single-event effects (SEEs) [1], are a significant concern for space-based electronics since they can lead to a loss of information, functional interruptions or, in the worst case, to a total loss of control of the spacecraft. SEEs are caused when energetic charged particles pass through the semiconductors and insulators that make up an integrated circuit (see Fig. 1(a)), liberating electrons from the constituent atoms and, in turn, potentially disturbing the normal operation of the circuit. The impact of ionization-induced SEEs has been traditionally assessed via exposure of the device to a heavy-ion beam or protons generated by a particle accelerator. However, since the introduction of optical approaches for simulating radiation effects on microelectronics [2], laser-based approaches have proven particularly well-suited for studying SEEs [3–6]. These pulsed-laser SEE (PL-SEE) approaches are attractive because they are laboratory-based, cost-effective, and permit carrier generation into well-defined locations in the device-under-test (DUT). PL-SEE testing that uses near-IR excitation (wavelengths > 1200 nm) exploits two-photon absorption (2PA) to generate

#379036 https://doi.org/10.1364/OE.27.037652
Journal © 2019 Received 30 Sep 2019; revised 18 Nov 2019; accepted 26 Nov 2019; published 12 Dec 2019

Optics EXPRESS

carriers following propagation through the back-side of the silicon (Si) wafer (see Fig. 1(a)) [7,8], thus avoiding optically opaque elements such as the packaging and metal overlayers, which are ubiquitous in modern microelectronics. Consequently, 2PA-based PL-SEE testing has become an essential tool owing to its ability to simulate the radiation effects associated with ionization with good spatial resolution in a cost-effective and timely manner.

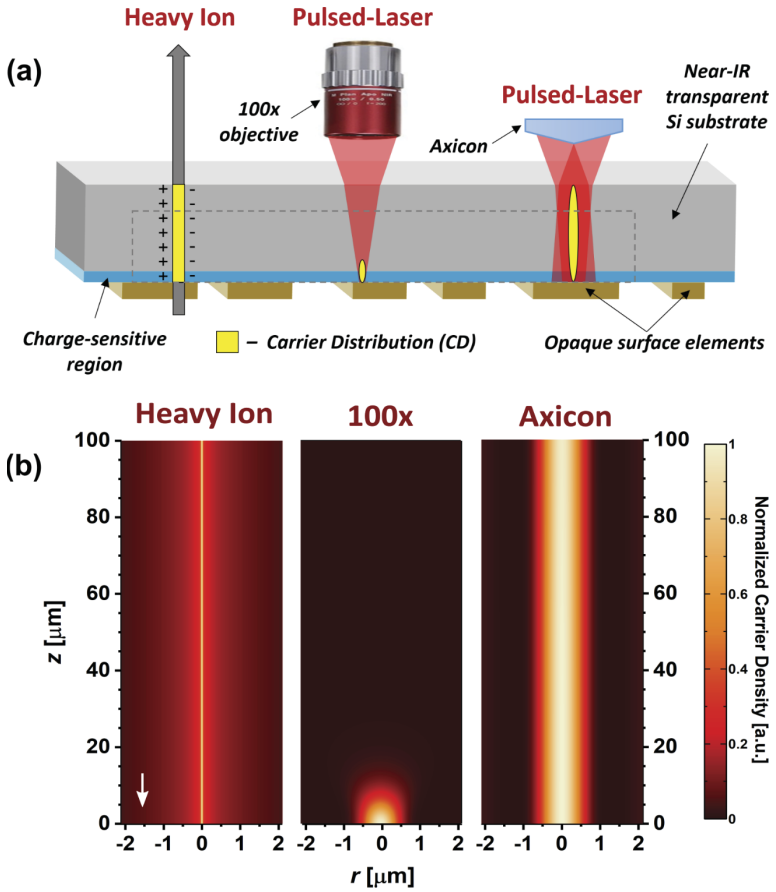

Fig. 1. Depiction of the carrier generation processes in a device or circuit (a). The region denoted by the dashed line represents the axial region in (b) where the carrier distributions (CDs) produced by each irradiation source are shown. The CDs are normalized to their respective peak carrier densities and the differences in the axial (z) and lateral (r) dimensions should be noted. The arrow denotes the direction of the irradiation from the back of the substrate to the charge-sensitive region. Since the CD produced by the heavy ion is narrower and possesses a larger peak carrier density than for the laser excitation, the carrier density is plotted on a log scale.

A primary goal of SEE testing is to *quantitatively* predict the effects of energetic particle radiation on microelectronics and, toward this end, the 2PA-based PL-SEE approach has been of limited utility. One of the main impediments to reaching this goal center around the 2PA-generated carrier distribution (CD). Since the CD generated by any excitation mechanism (proton, α-particle, x-ray, heavy ion, or laser) plays a critical role in determining the response of the device or circuit, an understanding of the magnitude and shape of this distribution is critical. Accurately quantifying the 2PA-generated CD is a complex, multidimensional problem. As depicted in Fig. 1(a), a microscope objective lens (e.g., 0.5 NA, 100x magnification) typically

Optics EXPRESS

is used to generate a micron-sized CD within the charge-sensitive region of the device. This tight focusing makes characterization of the pulse delivered to the DUT challenging and, given the quadratic dependence of the CD on the pulse intensity (see Section 3), this characterization must be accurate. Furthermore, there are difficulties associated with accurately modeling this generation process in Si (which typically makes up the charge-sensitive region for most commercial devices), including non-paraxial focusing conditions, complicated changes in beam shape during propagation, and optical aberrations induced at the surface of the semiconductor. Significant efforts have been devoted to pulse characterization [9] and numerical modeling [10] to verify that accurate determination of the 2PA-generated CD is possible [11]. Even with these advances, the most significant impediment to correlating laser and heavy-ion results remains the disparate shapes of the CDs generated by the radiation sources, coupled with how these CDs map onto the structure of the DUT. Since the interaction between the charge-sensitive region of the DUT and the CD dictates the device response, CDs with very different profiles can produce responses that are difficult, if not impossible, to correlate. A typical heavy-ion CD possesses an axial size that can exceed 100 μm, with a sub-micron lateral size, and so aspect ratios of >1000:1 are not uncommon. By contrast, a 2PA-generated CD produced with a 100x objective possesses a lateral size of ~1 μm and an aspect ratio of ~10:1. The drastic differences in the CDs can be seen in Fig. 1(b). Due to diffraction, any attempt to elongate the laser-generated CD to match that of a heavy ion comes at the expense of lateral resolution. While recent efforts have shown progress toward correlating results from these two irradiation sources [12,13], these approaches are still fundamentally limited by the differences in the carrier generation profiles.

In order to avoid these limitations, and to produce a carrier generation profile that better mimics that of a heavy ion, we propose the use of quasi-Bessel beams (QBBs) for 2PA-based PL-SEE testing. Bessel beams are non-diffracting light beams, which are characterized by a central lobe with an intensity and radius that is propagation invariant [14,15]. In practice, QBBs are propagation invariant only over a finite distance, but can still achieve micron-sized beams with aspect ratios that exceed 1000:1 [16]. These characteristics make QBBs attractive alternatives to traditional Gaussian beams, and have been exploited for many applications including microfabrication [16,17], nonlinear microscopy [18,19], multiphoton lithography [20], optical tweezers [21], optical coherence tomography [22,23], and quantum information processing [24]. These same features suggest that utilizing a QBB could better facilitate comparisons with heavy-ion testing. Figure 1(a) shows how a QBB can be produced using an axicon, or conical lens, in a PL-SEE setup. By using near-IR laser light, the QBB generates an elongated CD via 2PA resulting in a profile that more closely resembles that of a heavy ion (see Fig. 1(b)).

In this paper, we investigate the use of a QBB in the context of 2PA-based PL-SEE testing to determine whether it can be employed to predict the effects of heavy ions in microelectronics. First, we discuss how the axicon is incorporated into the optical layout for PL-SEE testing to produce the QBB. Second, we present the analytic equations that describe the 2PA-induced CD in a simple and intuitive form. Next, we detail a novel approach for directly characterizing the three-dimensional CD and show that the analytic equations can quantitatively determine the charge produced in a Si photodiode. Finally, we detail how the transient response of the photodiode from heavy-ion excitation is reproduced by the QBB by tuning the laser pulse energy to match the ion's charge deposition rate. A companion paper [25] discusses the radiation effects implications of this work in greater detail.

2. Modifications to 2PA-based PL-SEE optical layout

The typical 2PA-based PL-SEE optical layout, shown in Fig. 2, has been described in detail previously [8,9,13] but will be summarized here to highlight the modifications required to incorporate the QBB. The optical layout is essentially a microscope designed for reflective imaging. Imaging is critical to identify the specific element of interest as a DUT may consist

Optics EXPRESS

of several discrete devices (e.g., transistors) or a complicated circuit. This is accomplished by sending near-IR lamp light through the objective (Mitutoyo, M-Plan-Apo-NIR 100x, 0.5 NA), which passes through the Si substrate, reflects off the device/circuit or the metal overlayers (see Fig. 1(a)), and is imaged onto an InGaAs camera. The laser used for generating the 2PA-induced CD is injected from the side via a beamsplitter situated directly above the objective. For the traditional setup, the lens and axicon shown in Fig. 2 are not present such that the input laser beam (ω_0, beam radius HW1/e^2) typically overfills the back aperture of the objective to produce the smallest focal spot size and CD. A portion of this beam is reflected and imaged onto the InGaAs camera, which provides the location of the focused beam on the DUT. The DUT is positioned using a three-dimensional translation stage to co-locate the element to be tested with respect to the focused beam. The laser source generates pulses of $\tau = 99$ fs (HW1/e) at a wavelength of $\lambda = 1.26$ µm operating at a repetition rate of 1 kHz. The pulse energy delivered to the DUT typically ranges from 0.1 nJ to 1 nJ. All pulse energies are measured directly before the DUT and so reflection losses must be applied prior to any simulation. The methods for accurately characterizing the optical pulse delivered to the DUT are described in [9,11]. Finally, the carriers generated in the charge-sensitive region of the DUT induce current transients, which are acquired using a high-speed digital oscilloscope. These transients exhibit amplitudes, widths, and temporal shapes that are not only unique to the element being tested but the CD as well. Consequently, these transients can be used for assessing the efficacy of PL-SEE testing in replicating heavy-ion results, which is the subject of Section 5. By temporally integrating the current transient, one can obtain the collected charge (CC). This value is important in the context of quantitative laser-ion correlation. Furthermore, it can be related to the CD and therefore provides a means of comparing experimental data with the analytic equations describing the CD (see Section 3). This comparison is investigated in Section 4.2.

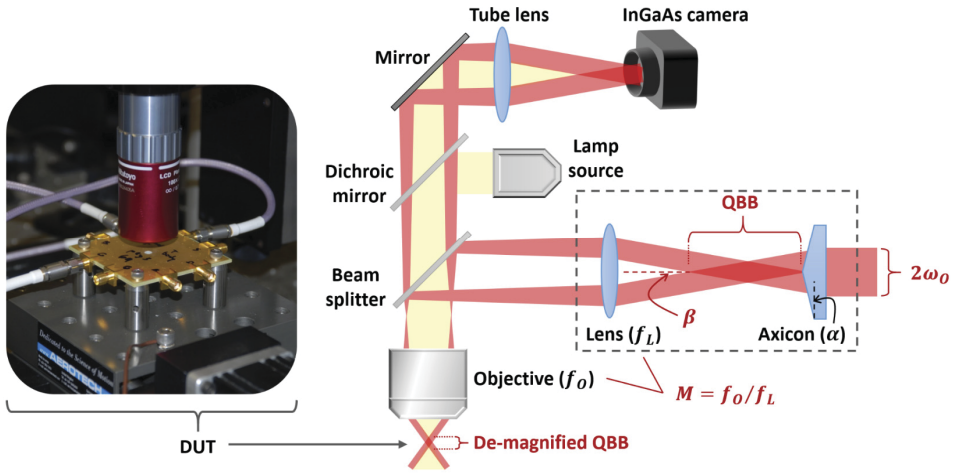

Fig. 2. Optical layout for 2PA-based PL-SEE testing. When the optical elements in the dashed box are not present, the traditional setup including excitation and imaging is represented. For the other setup, the incident laser beam and axicon generate the QBB, which is de-magnified by a telescope consisting of the lens (focal length f_L) and objective (focal length f_O). The resulting QBB is used to generate the CD in the DUT.

Axicons are commonly used to produce QBBs since they are inexpensive and provide high throughput [17,23,26]. The axicon's conical surface, defined by its base angle (α), causes different portions of the incident beam to interfere along the optical axis giving rise to the QBB. The angle that the refracted rays make with the optical axis is given by $\beta = \arcsin(n_a \sin\alpha) - \alpha$ (see Fig. 2), where n_a is the refractive index of the axicon. Generating the QBB in a PL-SEE

Optics EXPRESS

setup cannot be accomplished by simply replacing the microscope objective with an axicon since the imaging capability would be lost. To incorporate the axicon into the setup, a 4-f geometry is employed (as shown in Fig. 2) where the lens following the axicon (focal length f_L) and the objective (focal length f_O) form a telescope with a de-magnification of $M = f_O/f_L$. This geometry relays the QBB formed directly after the axicon to the position of the DUT, which is situated at the working distance of the objective. A number of benefits come from this layout: (*i*) imaging of the DUT is possible, (*ii*) the initial QBB is de-magnified such that micron-sized beams can be achieved while avoiding fabrication tolerance issues associated with large base-angle axicons [17,26], and (*iii*) simply removing the axicon and lens yields the traditional PL-SEE layout thus facilitating comparison between the two layouts. The specific geometry employed in this work consists of an input beam with $\omega_0 = 1.2$ mm, the axicon (Thorlabs, AX255, $\alpha = 5°$, $n_a = 1.45$, $\beta = 2.3°$), the lens (Thorlabs, LBF254-075, $f_L = 75$ mm), and the objective (Mitutoyo, M-Plan-Apo-NIR 20x, 0.5 NA, $f_O = 10$ mm), which gives a de-magnification of $M = 0.13$. The components were chosen to produce a QBB with suitable lateral and axial dimensions for PL-SEE testing and to make sure that the ring formed after the lens is not clipped or obstructed by the back aperture of the objective. The pulse energy and pulse width characterization are performed in an identical manner to traditional PL-SEE testing [9,11]. Generally, the pulse energies used for the QBB geometry are 10-20 times larger than for the traditional TPA testing geometry due to the larger aspect ratio of the CD. Pulse durations are not expected to be modified by the QBB geometry [27]. Finally, characterization of the spatial distribution of the QBB is described in Section 4.

The relevant parameters needed to describe the QBB are its lateral radius (R_B) and its axial length (L_B); the relationship between these parameters and the resulting CD are discussed in Section 3. For the QBB formed directly after the axicon, R_B and L_B depend only on the refraction angle β and the input beam radius ω_0 [23]. However, the introduction of the telescope affects these values as follows [26]: $\beta_M = \beta/M$ and $\omega_M = M\omega_0$. Essentially, the telescope creates a virtual axicon in front of the DUT [17], where the de-magnification results in an increase in the refraction angle and a decrease in the input beam size. With these modified values, the equations for R_B and L_B become

$$R_B = \frac{2.4048}{k_0 \tan(\beta_M/n_0)} \tag{1}$$

$$L_B = \frac{\omega_M}{\tan(\beta_M/n_0)} \tag{2}$$

where the wavevector $k_0 = 2\pi n_0/\lambda$ and n_0 is the index of Si (assumed to be 3.5 at $\lambda = 1.26$ μm). The material index is included to account for the reduction in the angle of refraction upon entering the DUT (depicted in Fig. 1). This reduction also ensures that these equations are valid since they are obtained under the small angle approximation [26]. With $M = 1$ and $n = 1$, Eqs. (1) and (2) reduce to the well-known formulae describing a QBB directly following an axicon [23]; for the geometry employed here, these calculations give $R_B = 12$ μm and $L_B = 30$ mm. A few dependencies can be gleaned from Eqs. (1) and (2). Compared to the QBB after the axicon, the QBB at the DUT has its R_B value decreased by M and its L_B value decreased by M^2. The impact of the index of Si is to elongate L_B by n_0, whereas the material has no impact on R_B since the refraction angle change is compensated by the wavevector change. Therefore, the calculated values inside the DUT for the geometry employed here are $R_B = 1.6$ μm and $L_B = 1900$ μm.

3. Expression for the 2PA-generated CD using a QBB

The intensity distribution of a QBB resulting from a Gaussian beam incident on an axicon (as shown in Fig. 2) has been reported previously [17,23,26]. Equation (3) reproduces this spatiotemporal distribution with modifications to make its interpretation clearer for the current

Optics EXPRESS

application:

$$I(r,z,t) = I_0 \cdot C_1 \cdot (z + L_B/2) \cdot e^{-2\left(\frac{z+L_B/2}{L_B}\right)^2} \cdot J_0^2\left(2.4048\frac{r}{R_B}\right) \cdot e^{-\left(\frac{t}{\tau}\right)^2}. \quad (3)$$

Here, $I_0 = \frac{2k_0E}{L_B\tau\sqrt{e\cdot\pi}}$ represents the peak intensity (*i.e.*, $I_0 = I(r = 0, z = 0, t = 0)$) where E is the pulse energy delivered to the charge-sensitive region of the DUT after accounting for Fresnel reflections off any intervening surfaces. The constant, $C_1 = \frac{2\sqrt{e}}{L_B}$, is introduced to normalize the rest of the expression. Equation (3) reveals a beam whose radial dependence is governed by a zeroth-order Bessel function (J_0) while its axial dependence is governed primarily by a Gaussian function [17,26]. A Gaussian temporal pulse shape is assumed. While this distribution describes a QBB produced directly after an axicon, the QBB within the DUT can be determined using the values of R_B and L_B from Eqs. (1) and (2), respectively. In order to verify that Eq. (3) accurately predicts the QBB within the DUT, the focusing of the light through the optical elements shown in Fig. 2 was modeled using optical simulation software (FRED, [28]) and the resulting intensity distribution showed near quantitative agreement with the analytic expression.

Under sufficiently strong intensities, a distribution of carriers, denoted as $N(r,z,t)$, can be generated via 2PA. The carrier generation rate is given by [8]

$$\frac{dN(r,z,t)}{dt} = \frac{1}{2}\frac{\beta_2 I(r,z,t)^2}{(hc/\lambda)} \quad (4)$$

where h is Planck's constant, c is the speed of light, and β_2 is the 2PA coefficient (the value of β_2 for Si at $\lambda = 1.26$ µm is taken to be 1.1×10^{-11} m/W [29]). Integrating Eq. (4) over all time results in the CD. For traditional 2PA PL-SEE testing, determining the CD requires the use of numerical calculations to account for the tight focusing of the laser beam [10]. Conversely, by using a non-diffracting QBB, these complications can be avoided. The expression for the 2PA-induced CD generated by a QBB is determined by simply substituting Eq. (3) in Eq. (4) and integrating over all time:

$$CD(r,z) = CD_0 \cdot C_2 \cdot (z + L_B/2)^2 \cdot e^{-4\left(\frac{z+L_B/2}{L_B}\right)^2} \cdot J_0^4\left(2.4048\frac{r}{R_B}\right). \quad (5)$$

Here, $CD_0 = \sqrt{\frac{2}{\pi}}\frac{k_0^2\beta_2\lambda E^2}{eL_B{}^2\tau hc}$ is the peak carrier density (*i.e.*, $CD_0 = CD(r = 0, z = 0)$) and $C_2 = \frac{4e}{L_B{}^2}$ is the normalization constant. As expected, the CD profile is very similar to the intensity profile of the QBB when accounting for the expected quadratic-dependence on intensity for a 2PA process.

Figure 3 plots the axial and radial dependencies of the 2PA-generated CD in Si from Eq. (5). The input parameters listed in the figure caption are identical to those used in Section 4 where the CD is experimentally characterized. Figure 3(a) shows the peak axial dependence, *i.e.*, $CD(r = 0, z)$, with $L_B = 1500$ µm. The length over which the carrier density remains within 10% of CD_0 is given as L_C. This can be considered an effective depth of field [26] and is a relevant parameter in the context of emulating a heavy-ion CD [25]. Figure 3(b) shows the peak radial dependence, *i.e.*, $CD(r, z = 0)$, with $R_B = 2$ µm. As a consequence of the quadratic dependence of the CD on intensity, the amplitudes of the first lobes are < 3% of CD_0. This ensures that the CD resulting from the QBB is essentially confined to the central peak and thus comparable to a heavy-ion CD. Finally, in addition to the values of L_B and R_B, the axial and radial FWHM values (ω_Z and ω_R, respectively) are also indicated on the plots since they provide a more intuitive measure of the distribution sizes [25].

Beam depletion due to 2PA depends on the intensity of the beam and the path length being traversed [30]. Generally, in 2PA-based PL-SEE testing, the beam must pass through the Si

Optics EXPRESS

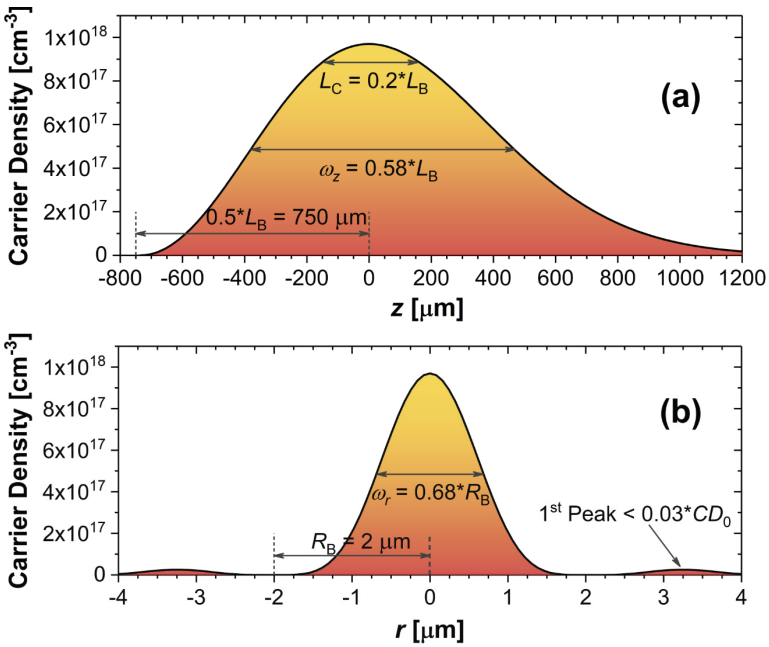

Fig. 3. Peak axial (a) and radial (b) profiles of the 2PA-generated CD in Si according to Eq. (5). The input parameters for the calculations are as follows: $E = 5.8$ nJ, $\tau = 99$ fs, $\lambda = 1.26$ µm, $n_0 = 3.5$, $\beta_2 = 1.1\times10^{-11}$ m/W, $L_B = 1500$ µm, $R_B = 2$ µm.

wafer (see Fig. 1), which is typically several hundreds of microns, and so beam depletion due to 2PA may be significant. Fortunately, the near-constant intensity of the QBB and the position of the charge-sensitive region implies that well-known equations for the transmittance loss (T_L) for a collimated beam [30] can be used. This factor can then be applied to the pulse energy E in Eq. (3) or Eq. (5) to account for the beam depletion. The depletion equation for a Gaussian pulse-shape and Gaussian beam-shape [30] would be most appropriate here (the central peak in Fig. 3(b) can be well-described by a Gaussian beam). However, inclusion of the pulse-shape results in a non-analytic expression and so, alternatively, the following equation is used:

$$T_L = \frac{\ln(1 + 0.63\ q_0)}{0.63\ q_0} \tag{6}$$

where $q_0 = \beta_2 I_0 L$, and L is the optical pathlength. Equation (6) is the same as the depletion equation for a CW, Gaussian beam [30] with a pre-factor of 0.63 included in front of q_0. As shown in Fig. 4, modification of this simple expression yields very good agreement with the non-analytic expression for a Gaussian pulse. The value of q_0 determines whether accounting for beam depletion is necessary (e.g., $q_0 < 0.2$ results in $T_L > 94\%$). For the calculations shown in Fig. 3 the peak intensity is $I_0 = 4.7\times10^{14}$ W/m^2; assuming a wafer thickness of $L = 400$ µm, a value of $T_L = 63\%$ is found ($q_0 = 2.1$). Given the quadratic-dependence of the CD on pulse energy, this would result in a 2.5× reduction in the CD_0 calculated in the absence of beam depletion. Clearly, depletion plays a large role in this case but, in other cases, it can prove to be negligible; the photodiode discussed in Section 4.2 is one such example.

Optics EXPRESS

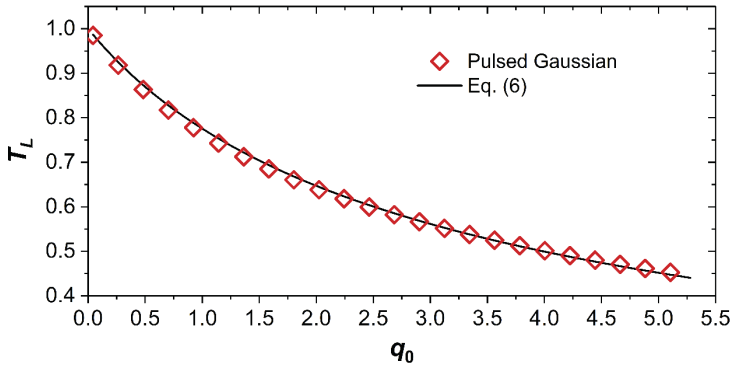

Fig. 4. Beam depletion due to 2PA calculated using a non-analytic expression [30] and the analytic expression given by Eq. (6).

4. Characterizing the CD and determining the generated charge

Accurately characterizing the three-dimensional CD generated by the QBB is critical for performing any quantitative analyses. Previous methods for characterizing the 2PA-generated CD include using microspheres (responsive to two-photon-induced fluorescence) to spatially sample the CD [19,26] and employing a Si CCD camera (responsive to two-photon-induced charge carriers) to profile the CD at different axial positions [17]. The approach taken here is to utilize devices, typical of those measured by PL-SEE testing, to characterize the CD. Such an approach requires no modification of the optical geometry, enables probing of the CD with high spatial resolution, and provides a means of comparing experimental data directly to the analytic expressions described in Section 3. Figure 5 illustrates how this comparison is made. A device under PL-SEE testing typically generates a current transient (acquired as a voltage transient on an oscilloscope) and temporal integration of this transient gives the CC. This value is related, through a collection efficiency (CE), to the amount of charge generated (Q_{SV}) within the sensitive volume (SV) of the device (see Fig. 1). Q_{SV} is related to the CD through a simple spatial integration over the SV. Importantly, if the SV is much smaller than the CD, Q_{SV} effectively samples the CD. This implies that the experimental observable, the CC, can be directly related to the analytic equations describing the CD. To sample the entire charge profile, CC values are acquired while the device is scanned across the CD. Therefore, axial and lateral CC scans can be fit to extract L_B and R_B, respectively, using Eq. (5).

4.1. Field effect transistor

The first device used to characterize the CD was a 45-nm n-type silicon-on-insulator (SOI) field effect transistor (FET). The details of this device are described elsewhere [25] but the critical characteristic of the FET is its very small SV. In the lateral dimension, the sensitive area is defined by the gate area and is $< 0.05\ \mu m^2$, significantly smaller than the CD. In the axial dimension, the sensitive depth (z_{SV}) is defined by the active layer, which is 80 nm; this ensures that the CD is sampled at a well-defined axial position. Accordingly, the experiments involved acquiring 50 drain transients per spatial position (for averaging purposes) as the FET was scanned across the QBB. The averaged CC values were found to be noisy due to the short transient durations ($<$ 200 ps). Alternatively, the averaged transient peak amplitudes were significantly quieter and therefore used for characterization. Since the transient shapes were found to be constant, the peak amplitudes should be proportional to the CC values and therefore reasonable for characterizing the CD.

Optics EXPRESS

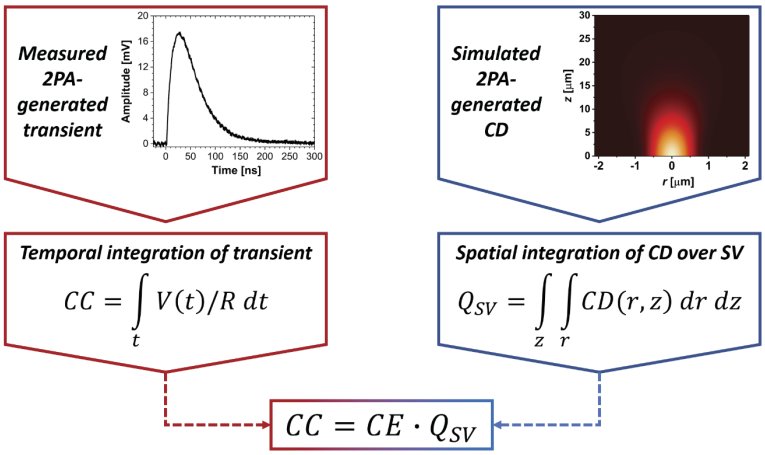

Fig. 5. Depiction of how transients measured during PL-SEE testing can be related to simulations of the 2PA-generated CD.

Lateral scans of the FET are shown in Fig. 6(a) for different axial positions. The scans are globally fit using the radial dependence of the CD (shown in Fig. 3(b)). The common width for all scans was found to be $R_B = 2.0\,\mu m$ ($\omega_R = 1.4$ μm). The good fits to the data and the constant width for different axial positions are both consistent with a QBB. The inset to Fig. 6(a) shows a 2-D raster (XY) scan of the FET, essentially extending the lateral scans to both spatial dimensions. This scan reveals a symmetric CD, as expected given the symmetry of the input beam. Although not shown here, scans over an extended lateral range did not reveal evidence of the first lobes shown in Fig. 3(b). Since these lobes should have amplitudes of ~3% of the amplitude of the main lobe, their presence is likely buried in the noise of the experiment. Fitting with the axial dependence of the CD (shown in Fig. 3(a)) should also be possible by performing an axial scan, or Z-scan, with the FET positioned at X = 0 μm, Y = 0 μm. When performing a Z-scan, the axial position of the DUT is multiplied by n_0 to account for the index modification of the focal position when inside Si. The Z-scan shown in Fig. 6(b) is fit reasonably-well with the axial dependence of the CD and reproduces the asymmetry in the scan (movement in the positive Z direction translates the DUT away from the objective). However, the extracted value of $L_B = 870\,\mu m$ ($\omega_Z = 500$ μm) is narrower than the axial profile shown in Fig. 3(a). This arises from difficulties in precisely aligning the micron sized QBB with the FET over several millimeters of stage movement, resulting in an artificial narrowing of the Z-scan. To address this, a large area, Si photodiode was utilized extract the axial dependence of the CD, as described below.

4.2. Si photodiode

The second device used for characterization is a large area, bulk, Si photodiode (Centronic OSD15-5T). The device has been tested extensively using both laser and heavy-ion excitation [12,31] and details of the device structure and testing conditions are described in [25]. For the current study, the photodiode possesses a very large sensitive area (> 14 mm^2). Consequently, while the lateral sampling resolution afforded by the FET is lost, the device is also insensitive to the lateral position of the QBB such that axial characterization can be performed more accurately. The value of the z_{SV} for the photodiode is 79 μm [25]; while this is significantly larger than for the FET, it is much smaller than the axial extent of the QBB and therefore appropriate for axial characterization. Z-scans for the photodiode (CC versus axial DUT position) are shown in Fig. 7 for two different pulse energies. The two curves show the expected quadratic dependence on pulse energy as determined for the CD in Eq. (5). Qualitatively, the scans look very similar to

Optics EXPRESS

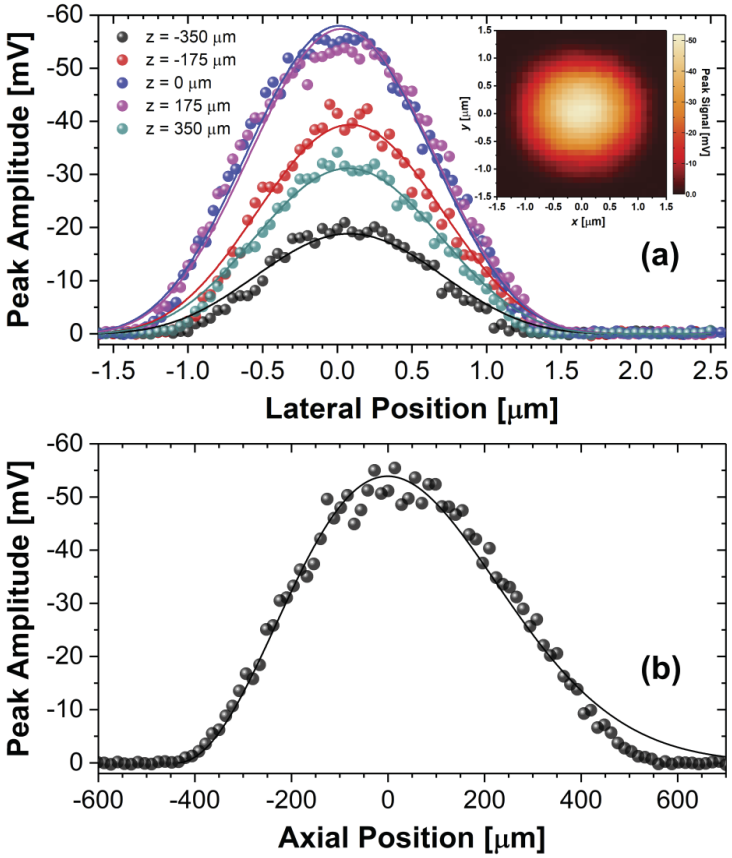

Fig. 6. Lateral (a) and axial (b) scans of the FET across the QBB. Icons represent experimental data of peak transient amplitude and the different curves in (a) are taken at different axial positions. Solid lines represent fittings of the data to the analytic expression for the CD given by Eq. (5). Extracted values are $L_B = 870$ μm and $R_B = 2$ μm. The inset to (a) is an XY raster scan of the QBB. The pulse energy measured before the DUT was 3.4 nJ.

the FET data in Fig. 6(b) but the value extracted from fitting with the CD axial dependence is considerably larger: $L_B = 1500$ μm ($\omega_Z = 870$ μm). The effective depth of field described above, or $L_C = 300$ μm, is equivalent to the region where the CC amplitudes are roughly constant in Fig. 7. Accurate spatial characterization of the QBB using the two devices results in values of $R_B = 2$ μm and $L_B = 1500$ μm. These values agree reasonably well (± 20%) with those estimated in Section 2 using only the input beam and the optical geometry.

With knowledge of the spatial characteristics of the QBB, quantitatively determining the 2PA-generated CD and, by extension, Q_{SV}, should be possible. In order to compare with experimental CC results, the collection efficiency (CE) must be known (see Fig. 5). For the photodiode discussed above, the CE has been shown to be 100% within the SV [12]; so, this device is ideal for determining whether the analytic expression for the CD can quantitatively predict experimental results. Q_{SV} is evaluated by integrating Eq. (5) over the SV of the photodiode. The axial integration limit is given by $z_{SV} = 79$ μm while the radial integration limit was chosen to be $r_{SV} = 6 \times R_B$ to account for the finite power carried in a QBB [32]. Using these integration limits and the parameters listed in Fig. 3, the value of Q_{SV} can be determined using Eq. (5). Two final points are important regarding the photodiode's impact on the value of the pulse energy (E).

Optics EXPRESS

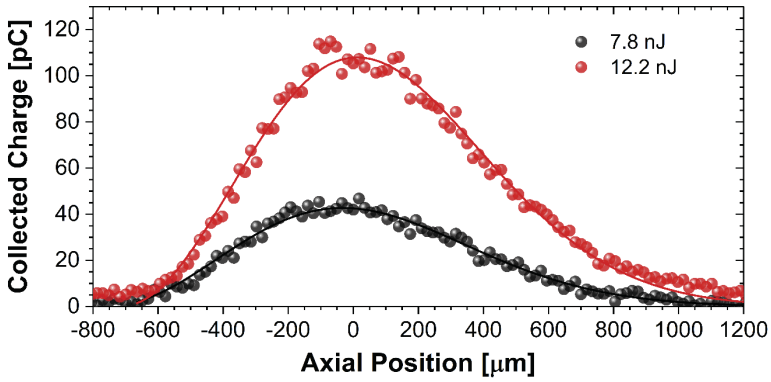

Fig. 7. Axial scans of the photodiode across the QBB for two different pulse energies. Icons represent experimental data of CC while solid lines represent fittings of the data to the analytic expression for the CD given by Eq. (5). The extracted value of L_B is 1500 μm. The pulse energies were measured before the DUT.

This device is studied via top-side excitation such that the beam does not pass through the Si substrate. Consequently, there is no need to account for beam depletion using Eq. (6). Also, the surface of the photodiode possesses a modest anti-reflection coating yielding reflection losses of 26% [12], which must be accounted for when determining E.

Figure 8 plots charge-collection data from the photodiode as a function of incident pulse energy. The pulse energy was varied using a waveplate-polarizer attenuator and the resulting transients were acquired and integrated to generate the CC values. For comparison, the values of Q_{SV} were

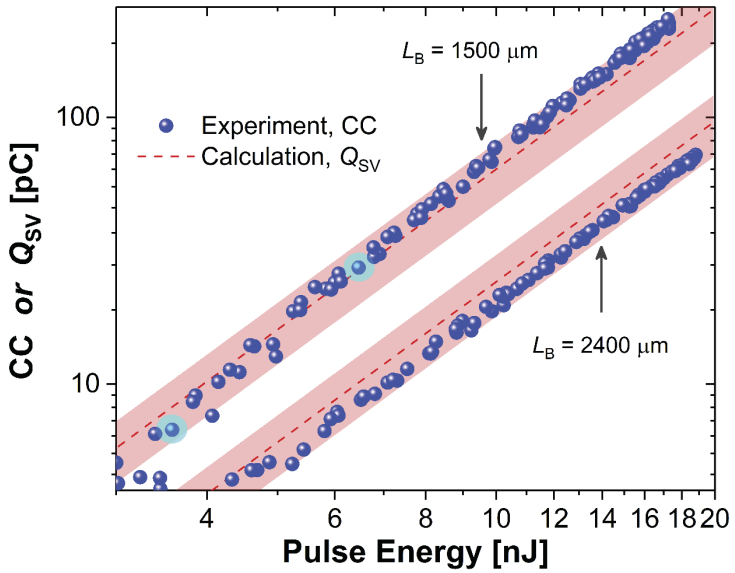

Fig. 8. Energy dependence of the CC data from the photodiode for QBBs with two different values of L_B. The calculated Q_{SV} values are determined from Eq. (5) and the shaded region denotes the error bars (+/- 26%) associated with the calculation. The pulse energies were measured before the DUT. The transients associated with the data points highlighted in light blue are used for comparison with heavy ion transients in Section 5.

Optics EXPRESS

calculated for these energies using Eq. (5). Errors in the calculated Q_{SV} values were estimated to be ± 26% based on uncertainties in the input parameters. There is strong quantitative agreement between the experimental data and the calculated values. It should be reiterated that the Q_{SV} values are derived from a simple analytic expression using only measured parameters (*i.e.*, no free-fitting parameters). While experiment/simulation agreement has been shown previously for traditional 2PA-based PL-SEE testing [11], the numerical simulations required for those are complicated owing to the non-paraxial focusing geometry. The diffraction-less QBB dramatically simplifies this calculation. Equation (5) is therefore capable of estimating the carriers generated by a QBB using 2PA, which could be useful in other applications such as determining the distribution of fluorophores for multiphoton microscopy [18,19], photoinitiator concentration for multiphoton lithography [20], or excited species for laser micromachining [16,17]. To the best of our knowledge, quantitative prediction of the QBB-generated CD has not been reported, likely because a proper vehicle for experimentally measuring it was not available. To further test the predictability of the analytic expression, the axial extent of the QBB was modified to a value of $L_B = 2400\,\mu m$ by changing the input beam to the axicon to $\omega_0 = 2.0\,mm$. The energy-dependent CC data are shown in Fig. 8 along with the calculated Q_{SV} values and the agreement between the experiment and simulation remains strong. Furthermore, from Eq. (5) it follows that $Q_{SV} \propto \frac{1}{L_B{}^2}$, and this is reflected in the data sets shown in Fig. 8, *i.e.*, a reduction in L_B by a factor of 1.6 gives an ~2.6× reduction in the CC.

5. Comparison of transients generated by a QBB and heavy ion

The ability to quantitatively calculate Q_{SV} for the photodiode makes it an ideal candidate for correlating laser data with heavy-ion data. Traditional 2PA-based PL-SEE testing on this device has shown some success in predicting heavy-ion results [12]. By ensuring that the values of Q_{SV} are equivalent for the two mechanisms, laser testing was able to accurately predict the CC generated by heavy-ion excitation. While predicting the CC (or the integral of the transient) is valuable, predicting the magnitude and shape of the transient is a critical goal in SEE testing. Using the traditional 2PA approach in [12], it was not possible to correlate transients produced by the two mechanisms. This is due to stark differences in the CDs produced by the two sources (see Fig. 1), which leads to different physical processes contributing to the transient [25].

In contrast, the similarity of the CDs produced by the QBB and the heavy ion should improve this correlation. Accordingly, heavy-ion testing was performed on the Si photodiode at Lawrence Berkeley National Laboratory and the details of these experiments are given in [25]. A heavy ion is generally described by a parameter known as its linear energy transfer (LET), or the rate at which it loses its energy as it passes through a material. Since this energy loss translates directly to the generation of charge, the LET can be expressed as a charge deposition rate in units of pC/μm. Figure 9 shows the photodiode transients produced by an argon ion and a krypton ion, which possess roughly constant LET values of 0.1 pC/μm and 0.32 pC/μm, respectively. In order to compare these data with QBB data, the laser-induced transients with equivalent charge deposition rates were selected from among the data shown in Fig. 8 (see highlighted points). Since deposited charge is essentially constant within the SV of the photodiode, the deposition rates are given by Q_{SV}/z_{SV}. For each heavy-ion transient, the respective QBB-generated transient shows strong agreement in terms of peak amplitude, shape and duration. By extension, this also implies that the CC values are highly correlated for the two mechanisms. Importantly, since Q_{SV} depends on the laser pulse energy, the charge deposition rate can be easily adjusted to match an LET associated with a specific heavy ion. Using this procedure, strong laser-ion correlation is achieved for transients generated by additional heavy ions [25]. Since transients exhibit complicated shapes unique to a device and CD, this agreement suggests that the QBB can emulate a heavy-ion response and therefore shows promise for predicting SEEs. It should be noted that the traditional 2PA approach has been used to successfully correlate laser and

Optics EXPRESS

heavy-ion transients in heterojunction bipolar transistors [13]. However, this correlation was achieved by using a weaker focusing geometry (*i.e.*, 20x objective versus 100x objective), which led to an axially elongated CD, but at the expense of lateral resolution. Since L_B and R_B can essentially be independently tuned, the QBB does not suffer from this restriction.

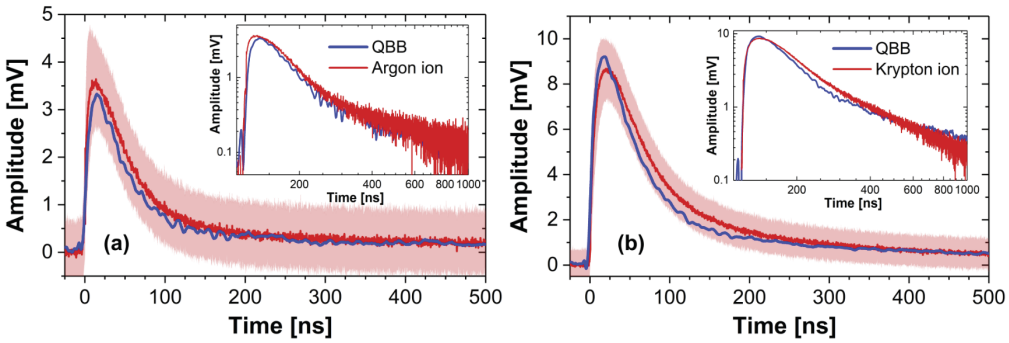

Fig. 9. Transients from the photodiode produced by the QBB and by a heavy ion. The charge deposition rates for the two excitation sources are matched in each figure.: 0.1 pC/μm (a) and 0.32 pC/μm (b). For the heavy-ion transients, the solid line represents the average of the measurements and the shaded region reveals the standard deviation. The insets reproduce the plots on a log-log scale to highlight the response at longer times.

6. Summary and conclusions

This work demonstrates that, by incorporating a QBB into a 2PA-based PL-SEE testing system, accurate prediction of SEE in a photodiode device is possible. This results not only from the heavy-ion-like CD created by the QBB, but also from a more simplified method for quantitatively determining the charge deposition. The QBB was generated in an existing PL-SEE setup through the introduction of just two elements: an axicon and a lens. Using devices typically measured by PL-SEE testing, *i.e.*, a 45-nm n-type SOI FET and a Si photodiode, the CD produced by the QBB was characterized with high spatial resolution revealing a charge profile similar to that of a heavy ion. Furthermore, the 2PA-generated CD can be described using a single analytic expression, which, despite its simplicity, is found to accurately estimate the 2PA-generated carriers based on its agreement with experimental charge-collection data. This ability to accurately determine the charge deposition permits a comparison of photodiode current transients produced by both the laser and by heavy ions under comparable conditions. For the photodiode, the transients from the two excitation mechanisms are found to be essentially identical, to within experimental error, representing a significant improvement over traditional 2PA-based laser testing for which such agreement generally is not possible. The ramification of this correlation is that, for this device, it is possible to predict the device response from heavy-ion excitation using a laser with its pulse energy tuned to the proper charge deposition rate. This novel approach retains all the benefits of traditional 2PA-based PL-SEE testing, but also may have utility as a predictive tool, which could substantially reduce the need for costly accelerator-based testing. Current investigations are aimed at expanding these efforts to study a wider range of device technologies to evaluate the predictive capability of this QBB approach.

Funding

Defense Threat Reduction Agency; Office of Naval Research.

Optics EXPRESS

Disclosures

The authors declare no conflicts of interest.

References

1. S. P. Buchner, F. Miller, V. Pouget, and D. McMorrow, "Pulsed-laser testing for single-event effects investigations," IEEE Trans. Nucl. Sci. **60**(3), 1852–1875 (2013).
2. D. H. Habing, "Use of lasers to simulate radiation-induced transients in semiconductor devices and circuits," IEEE Trans. Nucl. Sci. **12**(5), 91–100 (1965).
3. D. McMorrow, J. S. Melinger, S. Buchner, T. Scott, R. D. Brown, and N. F. Haddad, "Application of a pulsed laser for evaluation and optimization of SEU-hard designs," IEEE Trans. Nucl. Sci. **47**(3), 559–565 (2000).
4. J. S. Melinger, D. McMorrow, A. B. Campbell, S. Buchner, L. H. Tran, A. R. Knudson, and W. R. Curtice, "Pulsed laser-induced single event upset and charge collection measurements as a function of optical penetration depth," J. Appl. Phys. **84**(2), 690–703 (1998).
5. S. C. Moss, S. D. LaLumondiere, J. R. Scarpulla, K. P. MacWilliams, W. R. Crain, and R. Koga, "Correlation of picosecond laser-induced latchup and energetic particle-induced latchup in CMOS test structures," IEEE Trans. Nucl. Sci. **42**(6), 1948–1956 (1995).
6. J. A. Pellish, R. A. Reed, D. McMorrow, J. S. Melinger, P. Jenkins, A. K. Sutton, R. M. Diestelhorst, S. D. Phillips, J. D. Cressler, V. Pouget, N. D. Pate, J. A. Kozub, M. H. Mendenhall, R. A. Weller, R. D. Schrimpf, P. W. Marshall, A. D. Tipton, and G. F. Niu, "Laser-induced current transients in silicon-germanium HBTs," IEEE Trans. Nucl. Sci. **55**(6), 2936–2942 (2008).
7. D. McMorrow, W. T. Lotshaw, J. S. Melinger, S. Buchner, Y. Boulghassoul, L. W. Massengill, and R. L. Pease, "Three-dimensional mapping of single-event effects using two photon absorption," IEEE Trans. Nucl. Sci. **50**(6), 2199–2207 (2003).
8. D. McMorrow, W. T. Lotshaw, J. S. Melinger, S. Buchner, and R. L. Pease, "Subbandgap laser-induced single event effects: Carrier generation via two-photon absorption," IEEE Trans. Nucl. Sci. **49**(6), 3002–3008 (2002).
9. A. Khachatrian, N. J. H. Roche, D. McMorrow, J. H. Warner, S. P. Buchner, and J. S. Melinger, "A dosimetry methodology for two-photon absorption induced single-event effects measurements," IEEE Trans. Nucl. Sci. **61**(6), 3416–3423 (2014).
10. J. M. Hales, A. Khachatrian, N. J.-H. Roche, J. H. Warner, S. P. Buchner, and D. McMorrow, "Simulation of laser-based two-photon absorption induced charge carrier generation in silicon," IEEE Trans. Nucl. Sci. **62**(4), 1550–1557 (2015).
11. J. M. Hales, N. J.-H. Roche, A. Khachatrian, D. McMorrow, S. P. Buchner, J. Warner, M. Turowski, K. Lilja, N. C. Hooten, E. X. Zhang, R. A. Reed, and R. D. Schrimpf, "Strong correlation between experiment and simulation for two-photon absorption induced carrier generation," IEEE Trans. Nucl. Sci. **64**(5), 1133–1136 (2017).
12. J. M. Hales, A. Khachatrian, S. Buchner, N. J. H. Roche, J. Warner, Z. E. Fleetwood, A. Ildefonso, J. D. Cressler, V. Ferlet-Cavrois, and D. McMorrow, "Experimental validation of an equivalent let approach for correlating heavy-ion and laser-induced charge deposition," IEEE Trans. Nucl. Sci. **65**(8), 1724–1733 (2018).
13. A. Ildefonso, Z. E. Fleetwood, G. N. Tzintzarov, J. M. Hales, D. Nergui, M. Frounchi, A. Khachatrian, S. Buchner, D. McMorrow, J. H. Warner, J. Harms, A. Erickson, K. Voss, V. Ferlet-Cavrois, and J. D. Cressler, "Optimizing optical parameters to facilitate correlation of laser- and heavy-ion-induced single-event transients in SiGe HBTs," IEEE Trans. Nucl. Sci. **66**(1), 359–367 (2019).
14. D. McGloin and K. Dholakia, "Bessel beams: diffraction in a new light," Contemp. Phys. **46**(1), 15–28 (2005).
15. M. Mazilu, D. J. Stevenson, F. Gunn-Moore, and K. Dholakia, "Light beats the spread: "non-diffracting" beams," Laser Photonics Rev. **4**(4), 529–547 (2010).
16. M. Duocastella and C. B. Arnold, "Bessel and annular beams for materials processing," Laser Photonics Rev. **6**(5), 607–621 (2012).
17. S. Mitra, M. Chanal, R. Clady, A. Mouskeftaras, and D. Grojo, "Millijoule femtosecond micro-Bessel beams for ultra-high aspect ratio machining," Appl. Opt. **54**(24), 7358–7365 (2015).
18. L. Gao, L. Shao, B. C. Chen, and E. Betzig, "3D live fluorescence imaging of cellular dynamics using Bessel beam plane illumination microscopy," Nat. Protoc. **9**(5), 1083–1101 (2014).
19. G. Theriault, M. Cottet, A. Castonguay, N. McCarthy, and Y. De Koninck, "Extended two-photon microscopy in live samples with Bessel beams: steadier focus, faster volume scans, and simpler stereoscopic imaging," Front. Cell. Neurosci. **8**, 139 (2014).
20. H. Cheng, C. Xia, M. Zhang, S. M. Kuebler, and X. M. Yu, "Fabrication of high-aspect-ratio structures using Bessel-beam-activated photopolymerization," Appl. Opt. **58**(13), D91–D97 (2019).
21. J. Arlt, V. Garces-Chavez, W. Sibbett, and K. Dholakia, "Optical micromanipulation using a Bessel light beam," Opt. Commun. **197**(4-6), 239–245 (2001).
22. K. S. Lee and L. P. Rolland, "Bessel beam spectral-domain high-resolution optical coherence tomography with micro-optic axicon providing extended focusing range," Opt. Lett. **33**(15), 1696–1698 (2008).
23. N. Weber, D. Spether, A. Seifert, and H. Zappe, "Highly compact imaging using Bessel beams generated by ultraminiaturized multi-micro-axicon systems," J. Opt. Soc. Am. A **29**(5), 808–816 (2012).

Optics EXPRESS

24. M. McLaren, M. Agnew, J. Leach, F. S. Roux, M. J. Padgett, R. W. Boyd, and A. Forbes, "Entangled bessel-gaussian beams," Opt. Express **20**(21), 23589–23597 (2012).
25. J. M. Hales, A. Khachatrian, S. Buchner, J. Warner, A. Ildefonso, G. N. Tzintzarov, D. Nergui, D. M. Monahan, S. D. LaLumondiere, W. T. Lotshaw, J. D. Cressler, and D. McMorrow, "New approach for pulsed-laser testing that mimics heavy-ion charge deposition profiles," *IEEE Trans. Nucl. Sci.*, https://ieeexplore.ieee.org/document/8887522.
26. G. Theriault, Y. De Koninck, and N. McCarthy, "Extended depth of field microscopy for rapid volumetric two-photon imaging," Opt. Express **21**(8), 10095–10104 (2013).
27. R. Grunwald, M. Bock, V. Kebbel, S. Huferath, U. Neumann, G. Steinmeyer, G. Stibenz, J. L. Neron, and M. Piche, "Ultrashort-pulsed truncated polychromatic Bessel-Gauss beams," Opt. Express **16**(2), 1077–1089 (2008).
28. L. Photon Engineering, "FRED Optical Engineering Software," https://photonengr.com/fred-software/, Accessed October, 2018.
29. J. M. Hales, S.-H. Chi, T. Allen, S. Benis, N. Munera, J. W. Perry, D. McMorrow, D. J. Hagan, and E. W. Van Stryland, "Third-order nonlinear optical coefficients of Si and GaAs in the near-infrared spectral region," in *Conference on Lasers and Electro-Optics*, 2018 OSA Technical Digest (online) (Optical Society of America, 2018), paper JTu2A.59.
30. R. L. Sutherland, *Handbook of Nonlinear Optics* (Marcel Dekker, 1996).
31. S. Buchner, N. Roche, J. Warner, D. McMorrow, F. Miller, S. Morand, V. Pouget, C. Larue, V. Ferlet-Cavrois, F. El Mamouni, H. Kettunen, P. Adell, G. Allen, and D. Aveline, "Comparison of single event transients generated at four pulsed-laser test facilities-NRL, IMS, EADS, JPL," IEEE Trans. Nucl. Sci. **59**(4), 988–998 (2012).
32. F. Gori, G. Guattari, and C. Padovani, "Bessel-Gauss beams," Opt. Commun. **64**(6), 491–495 (1987).